

Ruiyu Sun * and Steven K. Krueger
University of Utah, Salt Lake City, Utah

1. Introduction

The DOE ARM program has promoted understanding of cumulus convection by producing high-quality “single-column model” observational datasets that allow one to run and evaluate single-column models and cloud-resolving models based on observed large-scale conditions (Xie and Zhang, 2000; Xie and Coauthors, 2002; Xu et al., 2002). The cloud and radiation fields produced by such simulations can then be compared to measurements by an ARM cloud profiling radar, as well as to satellite-based measurements (Luo et al., 2003; Luo and Krueger, 2004, 2005; Yang et al., 2006). This is an excellent evaluation method for stratiform cloud systems, but not for convective cloud systems, whose updrafts and downdrafts are inadequately sampled by the cloud profiling radars, and not detectable from space except by the TRMM precipitation radar, which has limited sampling at a given location (daily at its northern limit of 36 deg latitude). However, the existing observational systems at the ARM Southern Great Plains (SGP) Atmospheric Climate Research Facility (ACRF) can be used to provide a much more extensive statistical characterization of updrafts and downdrafts in convective cloud systems. The relevant datasets include the 5-minute Oklahoma Mesonet data and the hourly Arkansas Basin River Forecast Center (ABRFC) gridded precipitation data. Because convective cloud systems generally have strong interactions with boundary layer circulations and thermodynamics, the boundary layer wind and thermodynamic fields contain a great deal of information about convective cloud systems.

We are trying to produce a number of datasets based on Oklahoma Mesonet data and gridded precipitation data for multiple warm seasons that should be very useful for evaluating cumulus parameterizations in GCMs, and also for evaluating the representation of cumulus convection and the boundary layer in cloud-resolving models (CRMs). As the first step, we report in this extended abstract our preliminary results about how to estimate the *mesonet-averaged* cloud base updraft and downdraft mass fluxes from the surface divergence field.

2. Data Sources

Two datasets are used in our analyses, the Oklahoma Mesonet dataset and the Arkansas-Red River Basin Forecast Center hourly-gridded precipitation dataset. The Oklahoma Mesonet (sponsored by University of Oklahoma and Oklahoma State) provides 5-minute averaged surface meteorological data in quality assured data files. The Oklahoma Mesonet network consists of over 100 automated observing stations located throughout the state. Data are available from 1/1/1994 to 4/21/2007 (present). Data used in the current analysis are from May to August, 1997 and 2000.

The Arkansas-Red River Basin Forecast Center (ABRFC) produces an hourly gridded (4 km × 4 km) precipitation amount over the river basin. This field is a combination of both WSR-88D Nexrad radar precipitation estimates and rain gauge reports. The ABRFC performs extensive quality control on these data. The data are used for the ARM constrained variational analysis. Data are available from 6/24/1994 to 4/27/2007 (present). Data used in the current analysis are also from May to August, 1997 and 2000.

The locations of the various data referred to above are shown in Fig. 1. The Oklahoma Mesonet region is about 5 deg in longitude by 3 deg in latitude in size. Evaluating GCMs using our proposed data products would be straightforward. In this report focus is given to the results produced based on data in 1997.

3. Method of Analysis and Preliminary Results

Our goal is to estimate the *mesonet-averaged* updraft and downdraft cloud-base mass fluxes, $M_{c,u}$ and $M_{c,d}$, from the *mesoscale* surface divergence field. The triangle method was used to calculate the mesoscale horizontal divergence field ($\text{div} \equiv \partial u / \partial x + \partial v / \partial y$) directly from the mesonet station wind measurements (Dubois and Spencer, 2005; Davies-Jones, 1993). Figure 2 shows the horizontal divergence obtained from the Oklahoma Mesonet station data for a fair weather day, while Figure 3 shows the same for a day with precipitation. In the figures, each triangle formed from 3 stations is colored according to its divergence value: blue indicates weak divergence (divergence > 0), purple indicates strong divergence ($> 10^{-4} \text{ s}^{-1}$), yellow indicates weak convergence (divergence < 0), and red

* Corresponding author address: Department of Meteorology, University of Utah, Salt Lake City, UT 84112. E-mail: rsun@met.utah.edu

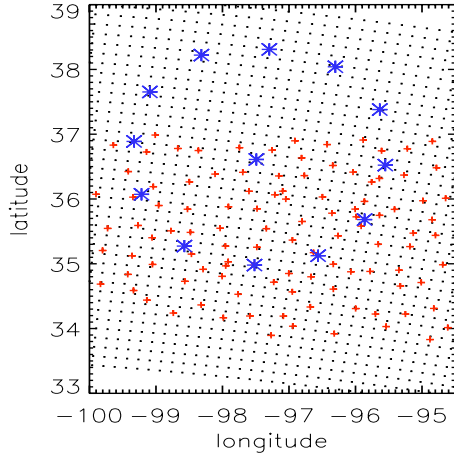


Figure 1: Map of SGP with every 4th grid point of the 4-km by 4-km hourly precipitation grid (dots), the Oklahoma Mesonet stations (red +), and constrained variational analysis domain (enclosed by blue stars). AERI profiles were retrieved at the Central Facility (central blue star) and at the blue stars at 12, 4, 6, and 8 o'clock.

indicates strong convergence ($> 10^{-4} \text{ s}^{-1}$). In Figure 3, the thick black contours delineate regions with precipitation rates greater than 2 mm h^{-1} .

When resolved at a scale of 100 m or less, the surface divergence field is obviously related to *boundary layer* updrafts and downdrafts because $\text{div} = -\partial w / \partial z$, neglecting density variations. If cloud-base updrafts and downdrafts are related to boundary layer updrafts and downdrafts, then we would expect that the surface divergence *averaged over regions of convergence only* ($\text{div} < 0$) would be related to $M_{c,u}$, and that the surface divergence *averaged over regions of divergence only* ($\text{div} > 0$) would be related to $M_{c,d}$.

The average station spacing of the Oklahoma Mesonet is about 30 km. This means that the mesonet very poorly resolves the divergence fields associated with individual boundary layer eddies. However, the mesonet can resolve to varying degrees the mesoscale circulations associated with cumulus and cumulonimbus clouds and with mesoscale convective systems. Therefore we define M_u , the mesonet analog of the surface divergence averaged over regions of convergence only, and M_d , the mesonet analog of the surface divergence averaged over regions of divergence only as

$$\begin{aligned} M_u &= \frac{-\sum_i A_i \text{div}_i H(-\text{div}_i)}{\sum_i A_i} \\ M_d &= \frac{\sum_i A_i \text{div}_i H(\text{div}_i)}{\sum_i A_i} \end{aligned} \quad (1)$$

where div_i is the horizontal divergence of the i th triangle, which has area A_i , and $H(x)$ is the Heaviside

step function.

M_u and M_d are typically nonzero due to convective boundary layer circulations even when there is no precipitating convection. Figure 2 is an example. Therefore, we also define M_u^+ , the mesonet surface divergence averaged over regions of convergence $> 10^{-4} \text{ s}^{-1}$, and M_d^+ , the mesonet surface divergence averaged over regions of divergence $> 10^{-4} \text{ s}^{-1}$. We have found that regions (triangles) with $|\text{div}_i| > 10^{-4} \text{ s}^{-1}$ tend to be associated with regions of precipitating convection. Figure 3 is an example. We calculated the time series of hourly values of M_u , M_d , M_u^+ , M_d^+ .

It is well known that convective downdrafts and cold pools tend to increase the variances of winds (u and v components), temperature (T), and water vapor mixing ratio (q) in the boundary layer (e.g., Zulauf and Krueger, 1997; Zulauf, 2001). Figure 4 shows a cold pool more than 100 km in diameter that was observed within the Oklahoma Mesonet. We used a 3D CRM simulation in a 128 km by 128 km domain with a 1-km horizontal grid size to compare the variances resolved by a mesonet with a 32-km grid with those resolved by the 1-km grid. Our results indicate the mesoscale grid resolves more than 90 percent of the variance during periods with mesoscale convective systems. We calculated the time series of hourly values of the mesonet variances of u , v , T , q , and of related quantities including moist static energy, $h \equiv c_p T + Lq + gz$.

We correlated the divergence-related time series with the time series of hourly area-averaged precipitation rate (P), which represents to some degree the cloud-base mass fluxes. Figure 5 shows the lagged correlations of P with M_d , M_u , M_u^+ , and M_d^+ , and standard deviations of moist static energy and wind obtained from the hourly times series for May–August 1997. The figure shows that (1) M_d , M_u , M_u^+ , and M_d^+ are correlated with P , (2) M_u^+ and M_d^+ are better correlated with P than are M_u and M_d , and (3) M_d and M_d^+ lag P and M_u and M_u^+ by about 1 h. These features are just what we would expect for convective precipitation and indicate that it is possible to retrieval cloud-base mass fluxes from surface divergence and other properties. The weak correlation between the standard deviation of h and P are mainly due to the contamination of the correlation by the variation of h induced by synoptical scale events and topographical effect.

4. Evaluation of the 'Retrieval' Method Using Model Simulation Data

We tested our cloud base-mass-fluxes 'retrieval' methodology by using results from a 54-hour simulation of maritime tropical convective cloud systems

Table 1: Least squares linear fit coefficients and RMS errors for $M_{c,u}$.

	A	B	RMS
M_u <i>true</i>	0.0059	940	0.0088
M_u <i>meso</i>	0.0061	1010	0.0094

Table 2: Least square linear fit coefficients and RMS errors for $M_{c,d}$.

	A	B	RMS
M_d <i>true</i>	0.0007	1030	0.0081
M_d <i>meso</i>	0.0007	1110	0.0084

observed during KWAJEX. The 3D simulation was performed with the UU LES with a horizontal grid size of 1 km and a horizontal domain size of 128 km by 128 km. We assumed that mesonet stations were located on a regular square grid with 32 km spacing.

Both updraft and and downdraft mass fluxes are calculated at 1050 m. Updraft mass flux occurs in cloudy grid cells with upward vertical velocity, while downdraft mass flux occurs in cloudy and/or precipitating grid cells with downward vertical velocity. Figure 8 shows the time series of cloud-base updraft and downdraft mass fluxes.

M_u and M_d are calculated at lowest model grid level (36 m) using (1). Two different methods are used to calculate div_i for each 32-km square. In the first method, u and v at all the points on the boundary of the 32-km square are used to calculate the true value of div_i for the square. In the second method, only u and v at the four corners of the 32-km square (representing mesonet stations) are used to estimate div_i . M_u and M_d calculated using the first method are called *true* M_u and M_d , represented by M_u *true* and M_d *true*. M_u and M_d calculated by using the second method are called *meso* M_u and M_d , represented by M_u *meso* and M_d *meso*. Large scale divergence is added to the true and meso div_i before true and meso M_u and M_d are calculated.

How well can we estimate $M_{c,u}$ and $M_{c,d}$ from true and meso M_u and M_d for a 32-km mesonet grid size? Figure 6 shows a scatter plot of both M_u *true* and M_u *meso* versus $M_{c,u}$. The correlation of $M_{c,u}$ and the M_u *true* is 0.82. The correlation of $M_{c,u}$ and M_u *meso* is 0.79. Figure 7 shows a scatter plot of both M_d *true* and M_d *meso* versus $M_{c,d}$. The correlations of $M_{c,d}$ and M_d *true* and M_u *meso* are 0.90 and 0.89, respectively. For comparison, the correlations of P and $M_{c,u}$ and $M_{c,d}$ are 0.77 and 0.93, respectively.

If we assume the following linear relationship between $M_{c,u}$ and M_u ,

$$M_{c,u} = A + BM_u, \quad (2)$$

then we obtain the coefficients A , B , and RMS error listed in Table 1. Similarly the coefficients and RMS error for the linear fit of $M_{c,d}$ using M_d are listed in Table 2. The differences in correlations and RMS errors between true and meso methods are small. The results strongly suggest that it is possible to estimate $M_{c,u}$ using either M_u *true* or M_u *meso*, and to estimate $M_{c,d}$ using either M_d *true* or M_d *meso*.

Figure 8 shows the time series of $M_{c,u}$ and $M_{c,d}$ at 1050 m and $M_{c,u}$ estimated using M_u *meso* and $M_{c,d}$ estimated using M_d *meso*. There is generally good agreement but with a slight time lag in the estimated values. Figure 9 shows the corresponding lagged correlations of P with $M_{c,u}$, $M_{c,d}$, M_d , and M_u . We see that M_u , M_d , and P lag the cloud-base updraft and downdraft mass fluxes, $M_{c,u}$ and $M_{c,d}$, by about 1 h on average, and that $M_{c,d}$ is more highly correlated with P than is $M_{c,u}$.

It is instructive to compare Fig. 9 with Fig. 5, which shows the lagged correlations of P with M_u and M_d obtained from the Oklahoma datasets. The most relevant aspect is that, taken together, these results imply that M_u and M_d are most correlated with $M_{c,u}$ and $M_{c,d}$ for lags of 1 to 2 h. We also see that both Oklahoma and KWAJEX have a maximum correlation between P and M_u at zero lag. However, the maximum correlation between P and M_d occurs at 1 h in Oklahoma, and at 0 h for KWAJEX. This difference is not surprising. There are several potential explanations. A good candidate is that the mesoscale cold pools that contribute to M_d are larger and more intense in Oklahoma, due to higher cloud bases and drier boundary layer air, and therefore M_d takes longer to maximize.

The maximum correlations between M_u and precipitation are similar for Oklahoma and KWAJEX (0.67 vs 0.69) but for M_d and precipitation, the correlation is significantly larger for KWAJEX (0.92 vs 0.70). These results suggest that the relationship between updrafts and precipitation may be more universal than that between downdrafts and precipitation.¹

5. Summary

Two observational datasets, the Oklahoma Mesonet data and the hourly ABRFC gridded precipitation data from May to August in 1997, were used to test the 'retrieval' of the *mesonet-averaged* cloud base updraft

¹The critical role of downdrafts in determining the structure of convective systems is well-known.

and downdraft mass fluxes from the surface divergence field. It is shown that (1) M_d , M_u , M_u^+ , and M_d^+ are correlated with P , (2) M_u^+ and M_d^+ are better correlated with P than are M_u and M_d , and (3) M_d and M_d^+ lag P and M_u and M_u^+ by about 1 h. This indicates that it is possible to retrieval cloud-base mass fluxes from surface divergence and other properties.

To examine how well this mass fluxes 'retrieval' method works data from a 54-hour CRM simulation of maritime tropical convective cloud systems observed during KWAJEX were used, along with the similar methods as in the Oklahoma Mesonet analysis. The results strongly suggest the possibility of estimates $M_{c,u}$ ($M_{c,d}$) using either M_u true (M_d true) or M_u meso (M_d meso). A generally good agreement was shown between the true and estimated $M_{c,u}$ ($M_{c,d}$) by using M_u meso (M_d meso). However there is a slight lag in the estimated values.

Since the CRM simulation was performed over ocean not land, the results from KWAJEX simulation analysis should be applied with caution over land. This might be one of the possible reasons why our defined M_u^+ and M_d^+ are not significantly better correlated with $M_{c,u}$ and $M_{c,d}$ than M_u and M_d do. Other possible reasons may include short simulation time and small simulation domain.

ACKNOWLEDGMENTS. This research was supported by the National Science Foundation Science and Technology Center for Multi-Scale Modeling of Atmospheric Processes, managed by Colorado State University under cooperative agreement No. ATM-0425247. James Kelly at the Australian Bureau of Meteorology provided the IDL code for the Barnes analysis.

References

- Barnes, S. L., 1994a: Applications of the Barnes objective analysis scheme Part I: Effects of undersampling, wave position, and station randomness. *J. Atmos. Oceanic Technol.*, **11**, 1433–1448.
- Barnes, S. L., 1994b: Applications of the Barnes objective analysis scheme Part II: Improving derivative estimates. *J. Atmos. Oceanic Technol.*, **11**, 1449–1458.
- Davies-Jones, R., 1993: Useful formulas for computing divergence, vorticity, and their errors from three or more stations. *Mon. Wea. Rev.*, **121**, 713–725.
- Dubois, J. A., and P. L. Spencer, 2005: Computing divergence from a surface network: Comparison of the triangle and pentagon methods. *Wea. Forecasting*, **20**, 596–608.
- Luo, Y., and S. K. Krueger, 2004: Cloud types simulated by the NCEP GFS single-column model. *Proceedings of the Fourteenth Atmospheric Radiation Measurement (ARM) Science Team Meeting*, U.S. Department of Energy, Albuquerque, NM, Extended Abstract: http://www.arm.gov/publications/proceedings/conf14/extended_abs/luo3-y.pdf.
- Luo, Y., and S. K. Krueger, 2005: Cloud properties simulated by a single-column model. Part 1: Comparison to cloud radar observations of cirrus clouds. *J. Atmos. Sci.*, **62**, 1428–1445.
- Luo, Y., S. K. Krueger, G. G. Mace, and K.-M. Xu, 2003: Cirrus cloud properties from a cloud-resolving model simulation compared to cloud radar observations. *J. Atmos. Sci.*, **60**, 510–525.
- Xie, S. C., and Coauthors, 2002: Intercomparison and evaluation of cumulus parameterizations under summertime midlatitude continental conditions. *Quart. J. Roy. Meteor. Soc.*, **128**, 1095–1136.
- Xie, S. C., and M. H. Zhang, 2000: Impact of the convection triggering function on single-column model simulations. *J. Geophys. Res.*, **105**, 14983–14996.
- Xu, K.-M., R. T. Cederwall, L. J. Donner, W. W. Grabowski, F. Guichard, D. E. Johnson, M. F. Khairoutdinov, S. K. Krueger, J. C. Petch, D. A. Randall, C. J. Seman, W.-K. Tao, D. Wang, S. C. Xie, J. J. Yio, and M.-H. Zhang, 2002: An intercomparison of cloud-resolving models with the Atmospheric Radiation Measurement summer 1997 Intensive Observation Period data. *Quart. J. Roy. Meteor. Soc.*, **128**, 593–624.
- Yang, F., H.-L. Pan, S. K. Krueger, S. Moorthi, and S. J. Lord, 2006: Evaluation of the NCEP Global Forecast System at the ARM SGP site. *Mon. Wea. Rev.*, **134**, 3668–3690.
- Zulauf, M. A., 2001: *Modeling the effects of boundary layer circulations generated by cumulus convection and leads on large-scale surface fluxes*. PhD thesis, University of Utah, Salt Lake City, UT 84112, 177 pp.
- Zulauf, M. A., and S. K. Krueger, 1997: Parameterization of mesoscale enhancement of large-scale surface fluxes over tropical oceans. *Preprints, 22nd Conf. on Hurricanes and Tropical Meteorology*, Fort Collins, CO. Amer. Met. Soc., 164–165.

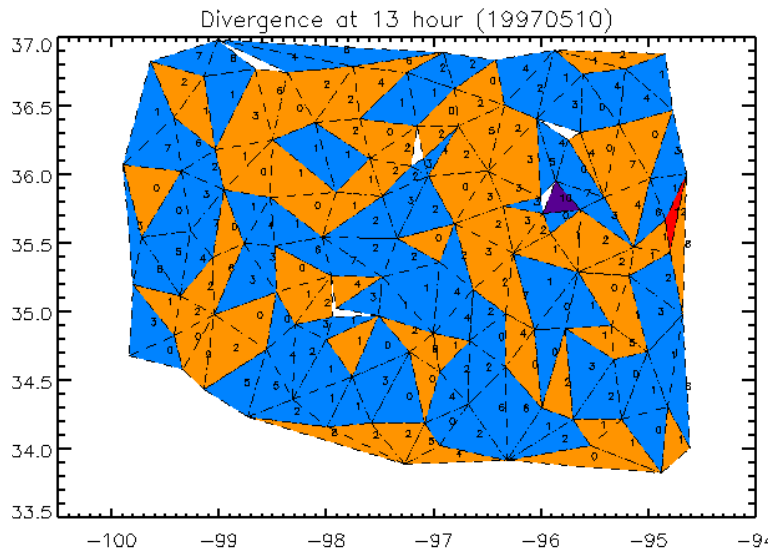


Figure 2: Divergence with colored triangles (see text for explanation; values are shown in units of 10^{-5} s^{-1}) and precipitation contours of 2 mm hr^{-1} (thick black line) at 13 UTC on May 10, 2007.

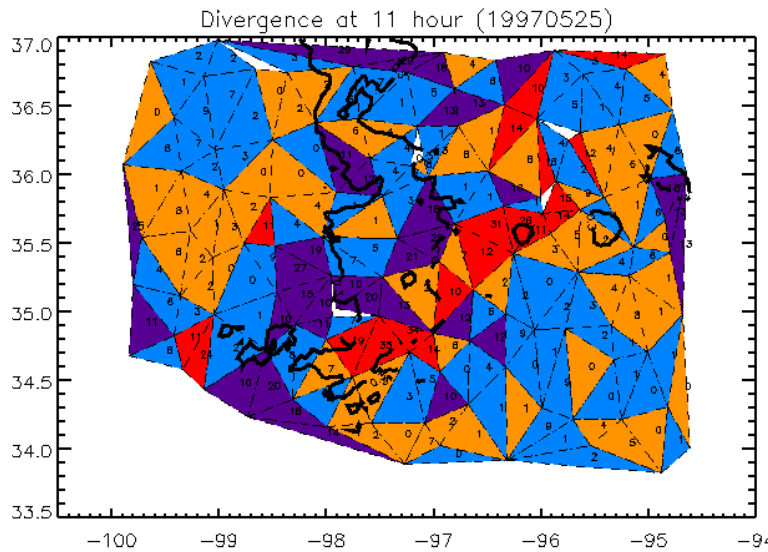


Figure 3: Divergence with colored triangles (see text for explanation; values are shown in units of 10^{-5} s^{-1}) overlaid with precipitation rate contours (2 mm hr^{-1}) at 11 UTC on May 25, 2007.

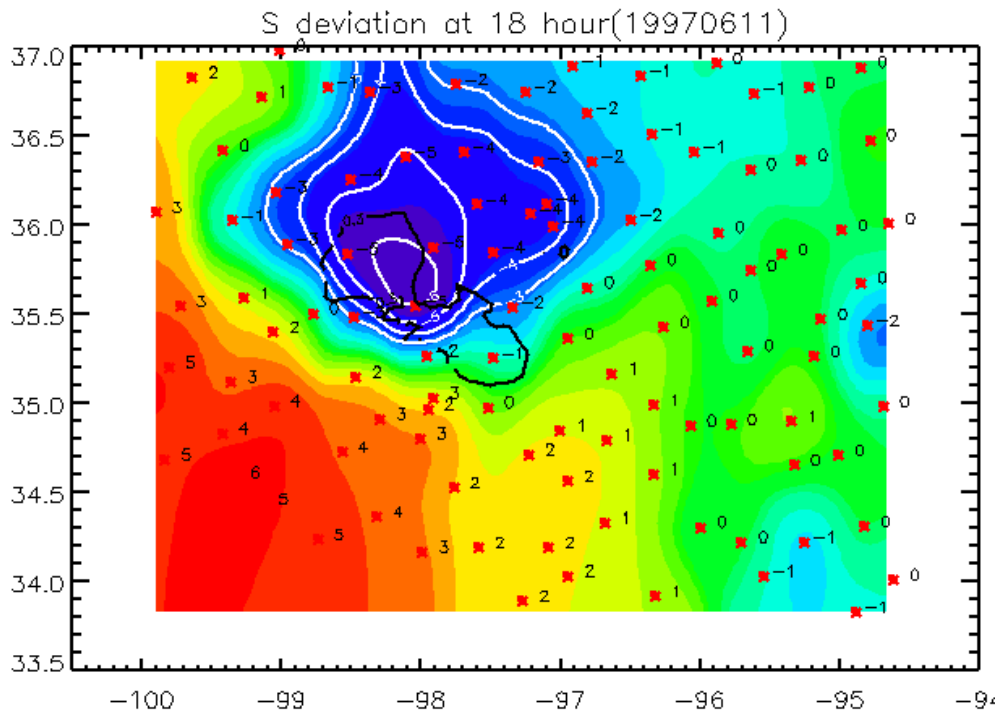


Figure 4: A cold pool represented by deviation of $s/c_p = T + gz/c_p$ (station values and white contours in K) from the Oklahoma Mesonet mean at 18 UTC, June 11, 1997. Precipitation rate (2 mm h^{-1}) contour is overlaid. Barnes (Barnes, 1994a,b) analysis was used to produce this figure.

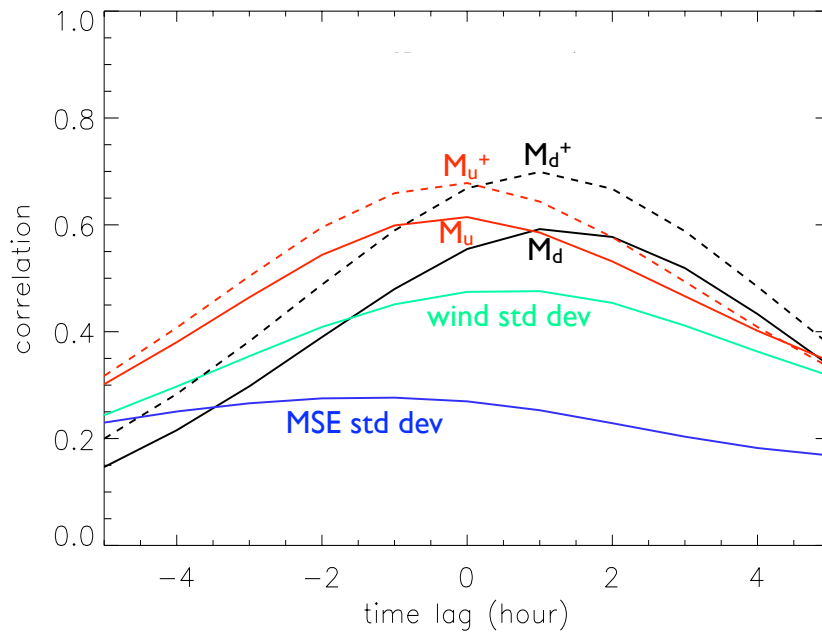


Figure 5: Lagged correlations of P with M_d , M_u , M_u^+ , M_d^+ , and standard deviations of moist static energy and wind for May–August 1997.

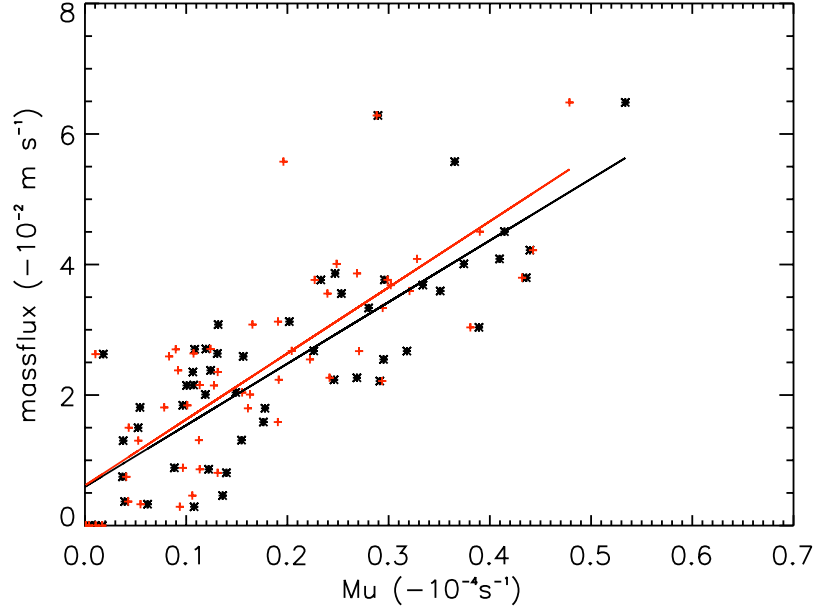


Figure 6: $M_{c,u}$ (m s^{-1}) at 1050 m AGL versus $M_u \text{ true}$ (black stars) and $M_u \text{ meso}$ (red crosses). Black and red lines are linear fits of $M_{c,u}$ and $M_u \text{ true}$ and $M_u \text{ meso}$.

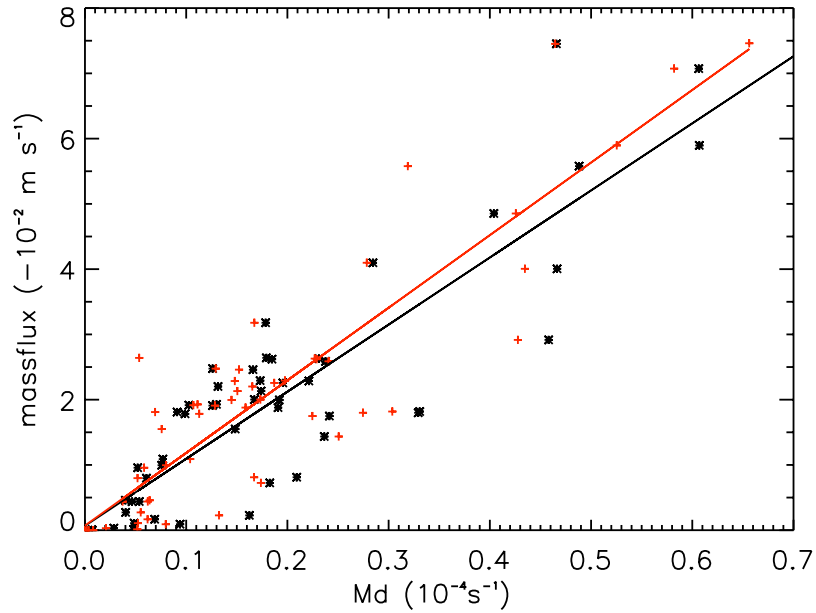


Figure 7: $M_{c,u}$ (m s^{-1}) at 1050 m AGL versus $M_d \text{ true}$ (black stars) and $M_d \text{ meso}$ (red crosses). Black and red lines are linear fits of $M_{c,d}$ and $M_d \text{ true}$ and $M_d \text{ meso}$.

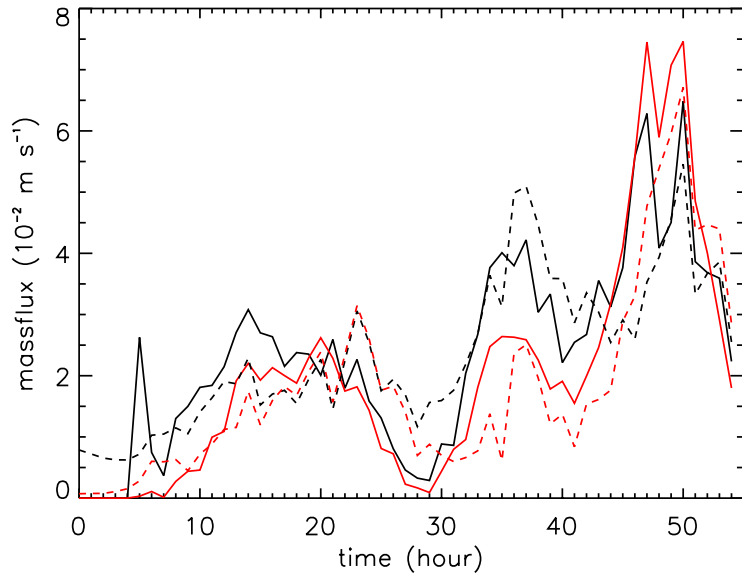


Figure 8: Time series of $M_{c,u}$ (black solid line) and $M_{c,d}$ (red solid line) at 1050 m AGL and $M_{c,u}$ estimated using $M_{u meso}$ (black dashed line) and $M_{c,d}$ estimated using $M_{d meso}$ (red dashed line).

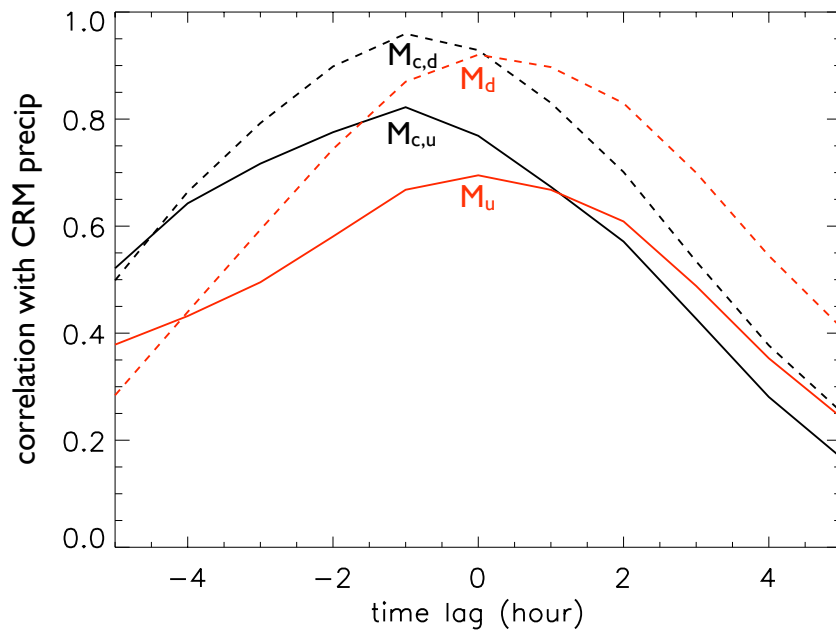


Figure 9: Lagged correlations of P with $M_{c,u}$, $M_{c,d}$, M_d , and M_u for the KWAJEX simulation.